# SWAP Gate for Spin Qubits Based on Silicon Devices Integrated with a Micromagnet

Ni, Ming; Ma, Rong Long; Kong, Zhen Zhen; Xue, Xiao; Zhu, Sheng Kai; Wang, Chu; Li, Ao Ran; Chu, Ning; Li, Hai Ou; More Authors

**DOI**
10.1021/acs.nanolett.4c05540

**Publication date**
2025

**Document Version**
Final published version

**Published in**
Nano Letters

NANO LETTERS

pubs.acs.org/NanoLett Letter

# SWAP Gate for Spin Qubits Based on Silicon Devices Integrated with a Micromagnet

Ming Ni,[¶] Rong-Long Ma,[¶] Zhen-Zhen Kong, Xiao Xue, Sheng-Kai Zhu, Chu Wang, Ao-Ran Li, Ning Chu, Wei-Zhu Liao, Gang Cao, Gui-Lei Wang, Xuedong Hu, Hong-Wen Jiang, Hai-Ou Li,* and Guo-Ping Guo

Cite This: *Nano Lett.* 2025, 25, 3766−3772 Read Online

ACCESS | Metrics & More | Article Recommendations | Supporting Information

**ABSTRACT:** In our toolbox of quantum gates for spin qubits, the SWAP-family gates based on Heisenberg exchange coupling are quite versatile: the SWAP gate can help solve the connectivity problem by realizing both short- and long-range spin state transfer, while the $\sqrt{\text{SWAP}}$ gate is a basic two-qubit entangling gate. Here we demonstrate a SWAP gate in a double quantum dot in isotopically enriched silicon in the presence of a micromagnet. We achieve a two-orders-of-magnitude adjustable ratio between the exchange coupling $J$ and the Zeeman energy difference $\Delta E_z$, overcoming a major obstacle for a high-fidelity SWAP gate. We also calibrate the single-qubit local phases, evaluate the logical-basis fidelity of the SWAP gate, and further analyze the dominant error sources. These results pave the way for high-fidelity SWAP gates and processes based on them, such as quantum communication on chip and quantum simulation.

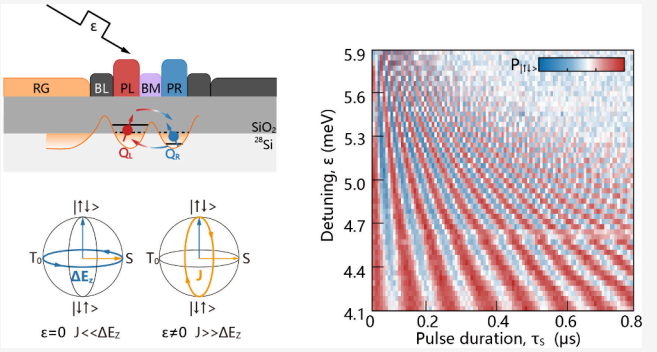


**KEYWORDS:** *quantum dot, Si-MOS, spin qubits, two-qubit gate, SWAP gate*



A single-spin qubit in a silicon quantum dot is an attractive platform for quantum information processing due to its long coherence times,[1−4] robustness against thermal noise,[5,6] and potential for scalability with advanced semiconductor manufacturing technology.[7−9] Rapid progress over the past years has seen high fidelity initialization,[10−13] readout,[12−15] single-qubit operation,[12,16,17] two-qubit operation,[18−21] and three-qubit iToffoli gate[22] successfully achieved, putting single-spin qubits at the threshold of demonstrating quantum error correction[22] and the noisy intermediate-scale quantum (NISQ) era.[23]

For a fault-tolerant and scalable quantum computer architecture, efficient quantum information transfer on a chip is essential. For a single-spin qubit in silicon, the transfer of the qubit state can be realized by shuttling the electron directly.[24−27] The SWAP gate, via the isotropic Heisenberg exchange coupling native between quantum dots, can transfer quantum information as suggested in the original spin qubit proposal.[28,29] the $\sqrt{\text{SWAP}}$ gate allows two-qubit entangling operations, and an extra SWAP gate can reduce circuit depth compared to using only the controlled-phase (CPhase) gate.[30] In short, for a large-scale spin qubit array, the SWAP gate is a crucial element for both quantum computing in general and on-chip communication in particular.

Although exchange control of spins has been demonstrated in GaAs quantum dots[31] and coupled donors,[32] demonstration of the SWAP gate remains a significant technical challenge for single-spin qubits in silicon quantum dots. For a high-fidelity SWAP gate, the main requirement is a highly adjustable ratio between the exchange coupling $J$ and the Zeeman energy difference $\Delta E_z$.[33] For devices with a micromagnet, with the gradient magnetic field designed to enable single-qubit addressability, the tunability of $J/\Delta E_z$ is limited by the field gradient and the resulting $\Delta E_z$.[34] For the device without the micromagnet, the tunability of $J/\Delta E_z$ is also limited due to the limited tunability of $J$.[28,35−37] While an equivalent to a SWAP gate can be constructed in a nonuniform magnetic field, such as the resonant SWAP gate, this more complex gate suffers from cross-talk[38] and heating, which significantly impact its applicability in large-scale qubit arrays. A recent work has demonstrated SWAP operation on a silicon double quantum dot (DQD),[37] though with only limited spin flip probability due to the finite tunability of $J/\Delta E_z$.

**Received:** November 4, 2024
**Revised:** January 26, 2025
**Accepted:** February 25, 2025
**Published:** February 28, 2025





https://doi.org/10.1021/acs.nanolett.4c05540
*Nano Lett.* 2025, 25, 3766−3772

In this article, we experimentally demonstrate a SWAP gate in an isotopically enriched silicon DQD with a built-in micromagnet and make suggestions on how to further enhance gate fidelity. In our experiment, while tuning the detuning $\varepsilon$, the exchange splitting $J$ increases/decreases rapidly while $\Delta E_z$ decreases/increases because of the spin−orbit coupling (SOC).[39] These opposite trends enable us to quickly adjust the ratio $J/\Delta E_z$ over more than 2 orders of magnitude and demonstrate a SWAP gate of high gate fidelity in theory. Using single-qubit gates, we are also able to calibrate local single-qubit phase shifts generated during the SWAP gate and provide a strategy to eliminate them completely. Utilizing independent spin readouts, we estimate the experimental logical-basis fidelity of the SWAP gate, analyze the main error sources, and estimate the actual gate fidelity in our experiment.

Our DQD two-qubit device (Figure 1(a-b)) is fabricated on a 70 nm $^{28}$Si epilayer with a residual $^{29}$Si concentration of 60 ppm[40−42] (see Supporting Information, S1). An external magnetic field $B_0$ = 605 mT is applied perpendicular to the interdot axis, as shown in Figure 1(b). A rectangular micromagnet on the top of the device enables electric dipole spin resonance (EDSR) by providing the slantzing magnetic field gradient ~0.06 mT/nm, which is one order smaller than the horseshoe geometry and causes a worse single-qubit operation quality (see Supporting Information, S5). Figure 1(c) shows the charge stability diagram of the DQD with charge occupancy ($N_L$, $N_R$).[43] Here we define the detuning $\varepsilon$ at the symmetric operation point as zero, which is located at point c in Figure 1(c). The pulsing path of the readout and initialization process is illustrated by the white arrows and colored dots in Figure 1(c)[44,45] (details in Supporting Information, S2).

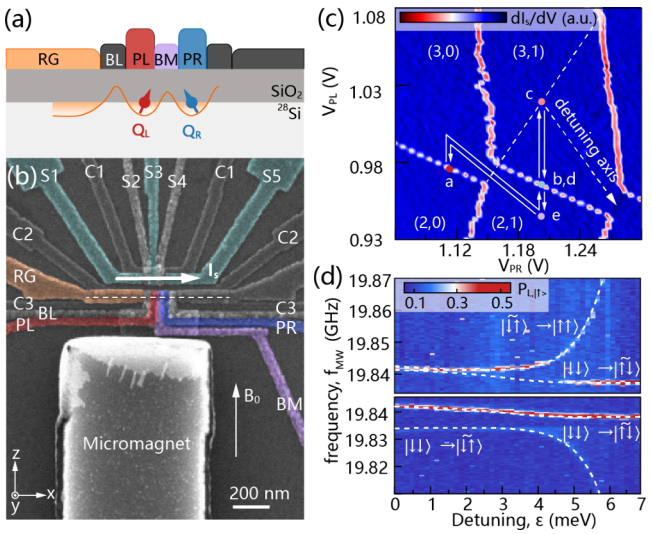


**Figure 1.** Two-qubit system and DQD spectrum. (a)-(b) Schematic and false-color scanning microscope image of a device identical to the one measured in the experiment. Schematic (a) illustrates the profile map along the white dotted line. (c) Charge stability diagram of the DQD formed underneath PL and PR. The different transition slopes of the right quantum dot are caused by the slow tunnel rate of the right quantum dot in the single reservoir device. Points a to e indicate the initialization, control, and readout positions. (d) DQD spectrum shows the spin-up probability of $Q_L$ versus the microwave frequency and the detuning $\varepsilon$ after initializing the system in $|\downarrow\tilde{\uparrow}\rangle$ (top) and $|\downarrow\downarrow\rangle$ (bottom) states. From the spectrum, we estimate $t_c$ = 1.5 GHz and the Stark shift near the symmetric operation point to be 128.6 MHz/V. The lever arm along the detuning axis is 0.14 meV/mV, which is extracted from the magneto-spectroscopy.

In this work we focus on the (3,1) - (2,2) region. In our single-reservoir device, the (3,1) - (2,2) configuration ensures that the electron wave functions have appropriate size for readout and gate operations. In this regime, the tunnel rate of both qubits can be suitable for Elzerman readout, while the tunnel coupling is proper for two-qubit gate operations. With two inner-shell electrons in the left dot remaining inert, the low-energy dynamics of the DQD are equivalent to those in the (1,1) - (0,2) regime. In the two-spin basis of ($|\uparrow\uparrow\rangle$, $|\uparrow\downarrow\rangle$, $|\downarrow\uparrow\rangle$, $|\downarrow\downarrow\rangle)^T$, a SWAP gate is given by the following unitary operator:

$$U_{\mathrm{SWAP}}(t) = \begin{pmatrix} 1 & & & \\ & \cos\left(\frac{\Delta E t}{2}\right) & \sin\left(\frac{\Delta E t}{2}\right) & \\ & \sin\left(\frac{\Delta E t}{2}\right) & \cos\left(\frac{\Delta E t}{2}\right) & \\ & & & 1 \end{pmatrix}$$

where $\Delta E = \sqrt{\Delta E_Z^2 + J^2}$ is the energy difference between the antiparallel eigenstates $|\downarrow\tilde{\uparrow}\rangle$ and $|\tilde{\uparrow}\downarrow\rangle$.

We first measure the energy spectrum of the two-qubit system. This is realized by pulsing the DQD to the symmetric operation point after preparing the system in the $|\downarrow\downarrow\rangle$ state and then modifying the detuning $\varepsilon$ diabatically. At various detuning $\varepsilon$, a frequency-chirped microwave pulse flips one of the spins. With an increased detuning $\varepsilon$, we plot the spin-up probability of $Q_L$ as a function of the microwave frequency in the bottom half of Figure 1(d). Two resonance peaks corresponding to the $|\downarrow\downarrow\rangle$ to $|\downarrow\tilde{\uparrow}\rangle$ and $|\downarrow\downarrow\rangle$ to $|\tilde{\uparrow}\downarrow\rangle$ transitions appear when the two qubits are in the $|\downarrow\downarrow\rangle$ state at the beginning. We can then prepare the qubits to $|\downarrow\tilde{\uparrow}\rangle$ with the extracted frequency and measure the resonance frequency corresponding to the $|\downarrow\tilde{\uparrow}\rangle - |\uparrow\uparrow\rangle$ transition while increasing the detuning $\varepsilon$. The result is shown in the top half of Figure 1(d). When we measure the energy spectrum, we readout the spin up probability of both $Q_L$ and $Q_L$. The results are given in Figure S8. With the extracted resonance frequencies, we can draw the energy-level structure schematic in Figure 2(a) and map the exchange interaction $J(\varepsilon)$, as well as $\Delta E(\varepsilon)$ and $\Delta E_z(\varepsilon)$, at different detuning $\varepsilon$, as shown in Figure 2(b). Notice that here $\Delta E(\varepsilon)$ and $J(\varepsilon)$ are directly measured, while the Zeeman energy difference is calculated from $\Delta E_z(\varepsilon) = \sqrt{\Delta E(\varepsilon)^2 - J(\varepsilon)^2}$. It is noteworthy that Figure 2(a) is an exaggerated depiction of the energy spectrum to clearly illustrate its structural characteristics and does not represent actual data values.

The DQD spectrum can be conveniently tuned electrically, which indicates the possibility of high tunability of $J/\Delta E_z$. When the detuning $\varepsilon$ is varied in the DQD by modifying gate voltage on each plunger gate, the electric field in the vicinity of the electron wave function also changes, which in turn modifies the qubit frequencies through an effective Stark shift. The effects of the intrinsic spin−orbit coupling (ISOC)[1,46−48] and the synthetic spin−orbit coupling (SSOC)[40,49] (the spin−orbit coupling brought by the micromagnet) are comparative, both


https://doi.org/10.1021/acs.nanolett.4c05540
Nano Lett. 2025, 25, 3766−3772

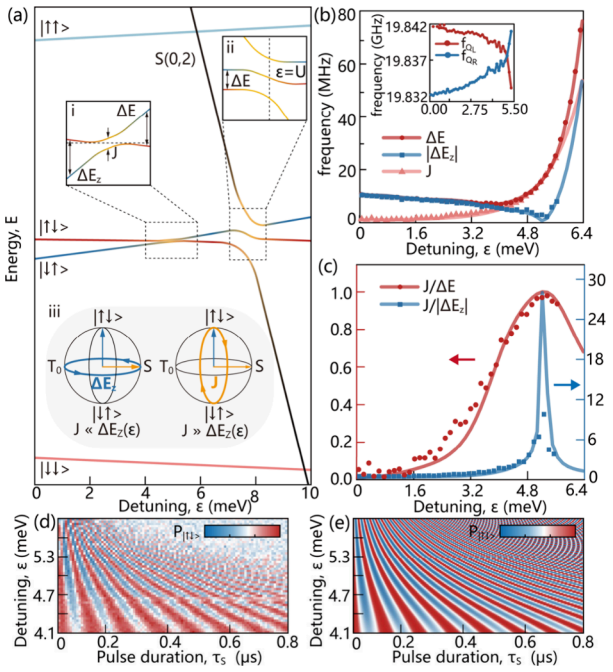


**Figure 2.** Energy-level structure. (a) Schematic of the energy-level structure of the two-electron spin states as functions of the detuning $\varepsilon$ between the (3,1) and (2,2) charge states. By exploiting the Stark shift, the energy levels of the two antiparallel spin states cross with each other (inset (i)). At the anticrossing between (3,1) and (2,2), the energy levels of the two antiparallel spin states shift by $J/2$ (inset (ii)). (b) $\Delta E_z$, $J$, and $\Delta E$ as functions of the detuning $\varepsilon$. The exchange interaction is fitted with $J \propto e^{\alpha\varepsilon}$, and $\Delta E_z$ is fitted with a fifth-order polynomial curve. With the influence of the Stark shift, the single-qubit resonant frequencies as a function of $\varepsilon$ are given in the inset. (c) Ratios $J/\Delta E$ and $J/|\Delta E_z|$ as functions of the detuning $\varepsilon$. The data without a fitting line can be found in Supporting Information Figure S9. (d-e) The measured and simulated probability of $|\uparrow\downarrow\rangle$ as a function of $\varepsilon$ and the pulse duration $\tau_s$ after preparing the two-qubit system to $|\uparrow\downarrow\rangle$.

of which are dependent on the quantum dot position (see Supporting Information, S6). In our device, an increase in $\varepsilon$ leads to a decrease in $\Delta E_z$. With the parameters in Figure 2(b), the ratios $J/|\Delta E_z|$ and $J/\Delta E$ as functions of detuning $\varepsilon$ are given in Figure 2(c). With increasing detuning $\varepsilon$, $J/|\Delta E_z|$ increases rapidly and reaches a sweet spot when $\Delta E_z$ equals zero, near which $J \gg \Delta E_z$ is easily satisfied. In our experiment, we find that ratio $J/|\Delta E_z|$ can be modified by $\varepsilon$ from 0.04 to 8.4, which is more than 2 orders of magnitude. To demonstrate a high-fidelity SWAP gate benefiting from the operation sweet spot, an implicit assumption here is that $\Delta E_z$ has to be smaller than a few tens of MHz at the symmetric operation point due to the limited adjusting ability of the effective Stark shift. Meanwhile, to increase the effect of the Stark shift, the ISOC part should be as large as possible,[46,47] and a smaller $b_{long}$ is preferred, which has the added benefit of improving single-qubit coherence.[16,50] The requirements on $\Delta E_z$ and the Stark shift can be satisfied for silicon quantum dot devices,[1,45−47,51] though further efforts are still needed to improve the micromagnet design,[49] substrate interface smoothness,[47] and control of the distance between quantum dots.[52] Here the barrier gate is not connected with the high bandwidth line and therefore cannot be pulsed to implement the SWAP gate. For the scenario of tuning the barrier gate, the SSOC will be more important than ISOC considering the location shift of the electron wave function. The micromagnet should be designed to give a higher longitude magnetic field gradient along the $x$-axis, while the single-qubit coherence will not be influenced. Moreover, for the platforms with strong spin−orbit coupling, such as hole spin qubits in Germanium, the ISOC will induce a stronger Stark shift; hence, there is more potential for realizing high-fidelity SWAP gates.

With a clear understanding of the energy spectrum of our DQD, we are ready to explore the two-electron dynamics of the system. First, we demonstrate the exchange oscillation, which underlies the SWAP gate, as shown in Figure 2(d). After initializing the system to the $|\downarrow\downarrow\rangle$ state at operation points a and b in Figure 1(c), an adiabatic microwave pulse with a 2 MHz chirp modulation[53] flips the state of $Q_L$ at operation point c. As illustrated in Figure 2(a) inset iii, when $\Delta E_z \gg J$, $|\uparrow\downarrow\rangle$ and $|\downarrow\uparrow\rangle$ are the eigenstates. Hence, the two qubits will be driven to the $|\uparrow\downarrow\rangle$ state at point c. After these single-qubit preparations, predistorted diabatic pulses[54] on gates PL and PR rapidly increase the detuning $\varepsilon$, which brings the system to the regime where $\Delta E_z \ll J$ while still maintaining the two-qubit state in $|\uparrow\downarrow\rangle$. When $\Delta E_z \ll J$, the eigenstates of the two-qubit system are the singlet−triplet (S-$T_0$) states, and the spin states of the two qubits will exchange with each other at a frequency $f_{ex} = \Delta E$. The exchange oscillation between the two antiparallel states as a function of $\varepsilon$ and the pulse duration $\tau_S$ is shown in Figure 2(d). We simulate the process by solving the time-dependent Schrödinger equation with $J(\varepsilon)$ and $\Delta E_z(\varepsilon)$ extracted from energy spectroscopy. The simulated exchange oscillation fringe shown in Figure 2(e) fits the experimental results quite well.

When we implement a SWAP gate with an exchange oscillation, the single-qubit local phases will inevitably accumulate, which could have direct consequences in a quantum circuit if not properly corrected. We find that there are two types of local phases for a SWAP gate (Supporting Information, S3). One part is "axis-dependent": it only depends on the starting moment of the SWAP gate, which makes the rotation axis of the SWAP gate rotate in the $x$−$y$ plane. It will accumulate at a frequency of $\Delta E_z$ at the symmetric operation point. Another part is "duration-dependent": it only depends on the pulse duration, which brings a Z-phase accumulation on each qubit. For the SWAP gate, only the duration-dependent part of the local phases can be compensated by a virtual Z-gate.[55,56] To eliminate the axis-dependent local phase, the idle time between the start time of the first single-qubit gate and the start time of the SWAP gate should ensure that the axis-dependent local phase equals to $2n\pi$ ($n$ = 1,2,3···).[57]

Due to the difficulties in driving $Q_L$ in this device (see Supporting Information, S5), we have designed a quantum circuit to demonstrate the existence of the axis-dependent local phase using only single-qubit operations on $Q_R$. As illustrated in Figure 3(a), in this quantum circuit, the axis-dependent local phase accumulated before the first SWAP gate was counteracted, and only the part that accumulated during the wait time remains. The spin-up-probability of $Q_R$ is read out, and the fitted oscillation frequency $f_{mp}$ = 7.90 MHz is very close to $\Delta E_z$ at zero detuning $\Delta E_z(0)$ = 7.73 MHz, which confirms the existence of the axis-dependent phase. To calibrate the duration-dependent local phase, we use a SWAP$^2$ operation rather than the SWAP operation for which the duration-dependent phase would be twice that of the SWAP operation. Compared to the measurement result without the SWAP$^2$


https://doi.org/10.1021/acs.nanolett.4c05540
Nano Lett. 2025, 25, 3766−3772

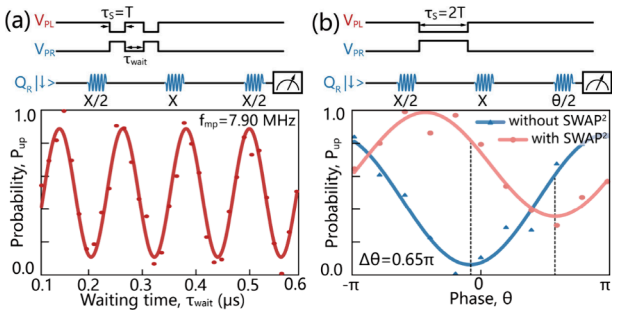


**Figure 3.** Local phase calibration. (a) The axis-dependent local phase accumulates as a function of waiting time $\tau_{wait}$. After initializing the qubits to the $|\downarrow\downarrow\rangle$ state, the diabatic pulse is inserted in an Hahn echo sequence, and the spin-up probability of $Q_R$ is read-out. Here, the pulse duration $\tau_S$ equals to the duration of a SWAP gate $T$. (b) The duration-dependent local phase of a SWAP$^2$ operation is calibrated by sweeping the phase of the latter $\frac{\pi}{2}$ rotation in an echo sequence. Here the pulse duration $\tau_s$ equals to $2T$.

operation, the extra local phase is $0.65\pi$, and it should equal to $2[(\omega - E_z) + d\omega]^*T$ (details in Supporting Information, S3), where $E_z$ and $\omega$ are the average Zeeman energies at the SWAP operation point and the single-qubit operation point (the symmetric point), respectively, and $d\omega$ is the Zeeman energy difference at the single-qubit operation point. From the DQD spectrum, the local phase can be theoretically calculated as $0.62\pi$, which matches the experimental result. Likewise, the local phase on $Q_L$ can be estimated as $-0.62\pi$.

To assess the fidelity of the SWAP gate, we first prepare the system in four different states $|\downarrow\downarrow\rangle$ ,$|\uparrow\downarrow\rangle$, $|\downarrow\uparrow\rangle$, and $|\uparrow\uparrow\rangle$ and then apply the exchange gate with pulse duration $\tau_s$. As $\tau_s$ increases, we observe the oscillation between $P_{|\uparrow\downarrow\rangle}$ and $P_{|\downarrow\uparrow\rangle}$ for the initial states $|\uparrow\downarrow\rangle$ and $|\downarrow\uparrow\rangle$, while $P_{|\downarrow\downarrow\rangle}$ and $P_{|\uparrow\uparrow\rangle}$ remain constant (Figure 4(a)). With the correlation between the input and output states, we can construct the truth table $M_{gate}$ (see Supporting Information, S2) with $\rho_{out} = M_{gate}(\rho_{in})$, which describes the linear map between the input and output states. It is worth noting that the truth table is not the operation matrix and thus cannot be used to calculate the gate fidelity directly. However, we can calculate the logical-basis fidelities[58,59] with it, which is defined as

$$F_{n\to f_n} = \frac{1}{N}\sum_{n=1}^{N} \langle f_n | M_{gate}(|n\rangle\langle n|) | f_n \rangle$$

Here $|n\rangle$ are the orthogonal input states, and $|f_n\rangle$ are the corresponding ideal output states. Both $|n\rangle$ and $|f_n\rangle$ are along the computational basis (ZZ axis here). The logical-basis fidelity, not the same as the operation fidelity, is a classical metric used to characterize the averaged probability of obtaining the correct output for each of the input states and can provide only the upper bound of the full operation fidelity in theory.[58] From our experimental measurements, the logical-basis fidelity of the gate operations is $F_{SWAP}$ = 82.3% ± 11.8% (see Supporting Information, S2). In our work, constrained by the lack of single-qubit control on $Q_L$, we can probe only the projection states and provide the classical fidelity. A more comprehensive and precise fidelity metric[13,18−21] would have been the better choice if all controls were available.

To analyze the effect of various error sources, we simulate a two-qubit system with the parameters extracted from the energy spectrum and calculate the influence of different error

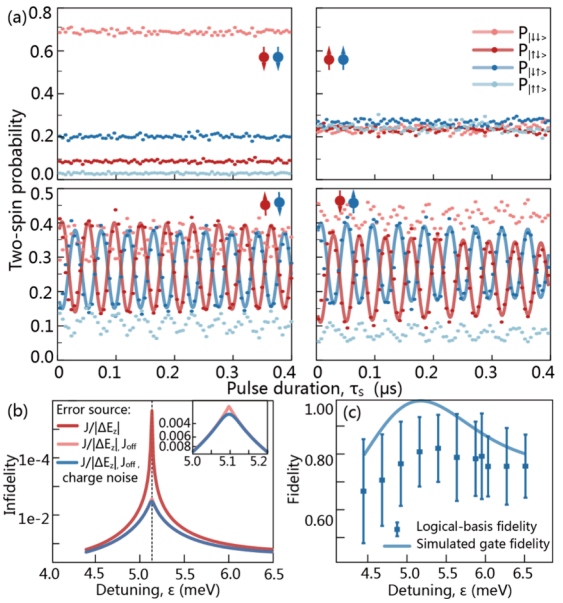


**Figure 4.** Gate fidelity and error source analysis. (a) The two-qubit probabilities as a function of $\tau_s$ with the initial state in $|\downarrow\downarrow\rangle$ $|\uparrow\downarrow\rangle$ $|\downarrow\uparrow\rangle$ and $|\uparrow\uparrow\rangle$, respectively. The solid lines fit to the oscillations of $P_{|\uparrow\downarrow\rangle}$ and $P_{|\downarrow\uparrow\rangle}$. (b) The infidelity of the SWAP gate as a function of $\varepsilon$. The colored curves indicate the simulated infidelities with different error sources included. (c) The logical-basis fidelity and simulated gate fidelity as a function of $\varepsilon$. The data points calculated from the truth tables.

sources, including $J/|\Delta E_z|$, finite $J_{off}$, and quasi-static charge noise. Quasi-static charge noise induces exchange oscillation decay through coupling with $\varepsilon$ and causes single-qubit frequency fluctuations, which degrade single-qubit operation quality via coupling with the gradient magnetic field.[60] Due to the lack of single-qubit operation characterization, for the quasi-static charge noise, we consider only the quasi-static[61,62] charge noise on $\varepsilon$, while we consider the charge noise coupling to the single qubit via the micromagnet as the unquantified error source. First, we incorporate coherent error sources $J/|\Delta E_z|$ and a finite $J_{off}$ into the simulation by using different Hamiltonians. The gate fidelity is calculated as $F_{gate} = tr(U^{\dagger}U_{ideal})$, where $U$ is the operator with errors and $U_{ideal}$ is the ideal gate operator (see Supporting Information, S4). As shown in Figure 4(b), the infidelity considering only finite $J/|\Delta E_z|$ is strongly dependent on detuning $\varepsilon$. This is evident because $J/|\Delta E_z|$ is a sensitive function of $\varepsilon$ and determines the rotation axis. Another error source is the nonvanishing exchange coupling $J_{off}$ at the idle point, which changes the eigenstates at the symmetric operation point, and the operation fidelity in the new basis is lower. Here we use $J_{off}$ = 0.8 MHz in our simulation, which is the value we have in the experiments. The result in Figure 4(b) shows that $J_{off}$ reduced the operation fidelity by 0.25% at the sweet spot operation point. The influence of charge noise is considered with respect to the gate fidelity via Monte Carlo simulation. The standard deviation $\sigma_\varepsilon$ of the charge noise can be acquired by reproducing the damping in the exchange oscillation decay (see Supporting Information, S3). The result indicates that the gate infidelity due to charge noise on $\varepsilon$ is about 0.05% (see Supporting Information, S4). This small contribution from charge noise on $\varepsilon$ is a direct result of the operation sweet spot, where $\Delta E_z$ = 0 MHz, with the operation point far from the


https://doi.org/10.1021/acs.nanolett.4c05540
Nano Lett. 2025, 25, 3766−3772

(3,1) - (2,2) anticrossing. Moreover, a fast gate operation speed also reduces the level of accumulation of the noise effect, leading to suppression of incoherent errors.

As shown in Figure 4(c), the tendency of the simulated gate fidelity fits well with the experimental result. For the coherent error sources, to realize the single-qubit gate and SWAP gate with a gate fidelity higher than 99% simultaneously, the ratio $\frac{J_{tr}}{dE_{tr}}$ at least must be tuned from lower than 0.1 to larger than 10 diabatically, where $J_{tr}$ and $dE_{tr}$ are the exchange coupling and the Zeeman energy difference in the new basis (see Supporting Information, S4). We ascribe the remaining deviation between the logical-basis fidelity and the simulated gate fidelity to the SPAM (spin preparation and measurement) error and the unaccounted charge noise coupling to the single qubit. The SPAM errors, including the cross-talk error of the single-shot readout and the initialization error, are not fully separated from the logical-basis fidelity, making it deviate from the theoretical upper limit value. The charge noise coupling to the single qubit should be further removed by an improved micromagnet or faster gate operation.

In summary, we demonstrate the native SWAP gate for spin qubits in a gate-defined DQD in isotopically purified $^{28}$Si. We implemented a strategy to calibrate and eliminate local phase shifts induced during the SWAP gate. The truth tables are measured to give logical-basis fidelity, and the influences of various error sources are analyzed to estimate and further improve the gate fidelity. The demonstration of adjustable $J/\Delta E_z$ indicates that a high-fidelity SWAP gate can be achieved even in the presence of a micromagnet, which can in turn facilitate on-chip quantum communication and act as an essential two-qubit gate for quantum information processing. Future experiments will focus on improving single-qubit operation quality, reducing SPAM errors, and optimizing the control pulse scheme, so that we can realize a high-fidelity SWAP gate even with a larger $\Delta E_z$.

## ■ ASSOCIATED CONTENT

### Supporting Information

The Supporting Information is available free of charge at https://pubs.acs.org/doi/10.1021/acs.nanolett.4c05540.

Device fabrication and experiment setup details; fidelity measurement, spin shuttling results, readout fidelity measurement and operation fidelity calculation; theory model of the SWAP gate; noise model and noise fitting details; single-qubit operation properties; analysis of the Stark Shift originations; and additional figures of the raw data of Figure 1b and Figure 2b,c (PDF)

## ■ AUTHOR INFORMATION


### Corresponding Author

**Hai-Ou Li** − *CAS Key Laboratory of Quantum Information, University of Science and Technology of China, Hefei, Anhui 230026, China; CAS Center for Excellence in Quantum Information and Quantum Physics, University of Science and Technology of China, Hefei, Anhui 230026, China; Hefei National Laboratory, University of Science and Technology of China, Hefei 230088, China;* orcid.org/0000-0002-9898-4735; Email: haiouli@ustc.edu.cn

### Authors

**Ming Ni** − *CAS Key Laboratory of Quantum Information, University of Science and Technology of China, Hefei, Anhui 230026, China; CAS Center for Excellence in Quantum Information and Quantum Physics, University of Science and Technology of China, Hefei, Anhui 230026, China*

**Rong-Long Ma** − *CAS Key Laboratory of Quantum Information, University of Science and Technology of China, Hefei, Anhui 230026, China; CAS Center for Excellence in Quantum Information and Quantum Physics, University of Science and Technology of China, Hefei, Anhui 230026, China*

**Zhen-Zhen Kong** − *Integrated Circuit Advanced Process R&D Center, Institute of Microelectronics, Chinese Academy of Sciences, Beijing 100029, China;* orcid.org/0000-0001-8563-5424

**Xiao Xue** − *QuTech and Kavli Institute of Nanoscience, Delft University of Technology, Delft 2628 CJ, The Netherlands*

**Sheng-Kai Zhu** − *CAS Key Laboratory of Quantum Information, University of Science and Technology of China, Hefei, Anhui 230026, China; CAS Center for Excellence in Quantum Information and Quantum Physics, University of Science and Technology of China, Hefei, Anhui 230026, China*

**Chu Wang** − *CAS Key Laboratory of Quantum Information, University of Science and Technology of China, Hefei, Anhui 230026, China; CAS Center for Excellence in Quantum Information and Quantum Physics, University of Science and Technology of China, Hefei, Anhui 230026, China*

**Ao-Ran Li** − *CAS Key Laboratory of Quantum Information, University of Science and Technology of China, Hefei, Anhui 230026, China; CAS Center for Excellence in Quantum Information and Quantum Physics, University of Science and Technology of China, Hefei, Anhui 230026, China*

**Ning Chu** − *CAS Key Laboratory of Quantum Information, University of Science and Technology of China, Hefei, Anhui 230026, China; CAS Center for Excellence in Quantum Information and Quantum Physics, University of Science and Technology of China, Hefei, Anhui 230026, China*

**Wei-Zhu Liao** − *CAS Key Laboratory of Quantum Information, University of Science and Technology of China, Hefei, Anhui 230026, China; CAS Center for Excellence in Quantum Information and Quantum Physics, University of Science and Technology of China, Hefei, Anhui 230026, China*

**Gang Cao** − *CAS Key Laboratory of Quantum Information, University of Science and Technology of China, Hefei, Anhui 230026, China; CAS Center for Excellence in Quantum Information and Quantum Physics, University of Science and Technology of China, Hefei, Anhui 230026, China; Hefei National Laboratory, University of Science and Technology of China, Hefei 230088, China;* orcid.org/0000-0002-3599-5496

**Gui-Lei Wang** − *Beijing Superstring Academy of Memory Technology, Beijing 100176, China; Hefei National Laboratory, University of Science and Technology of China, Hefei 230088, China*

**Xuedong Hu** − *Department of Physics, University at Buffalo, SUNY, Buffalo, New York 14260, United States*

**Hong-Wen Jiang** − *Department of Physics and Astronomy, University of California, Los Angeles, California 90095, United States*

**Guo-Ping Guo** − *CAS Key Laboratory of Quantum Information, University of Science and Technology of China, Hefei, Anhui 230026, China; CAS Center for Excellence in Quantum Information and Quantum Physics, University of*




https://doi.org/10.1021/acs.nanolett.4c05540
Nano Lett. 2025, 25, 3766−3772

*Science and Technology of China, Hefei, Anhui 230026, China; Hefei National Laboratory, University of Science and Technology of China, Hefei 230088, China; Origin Quantum Computing Company Limited, Hefei, Anhui 230088, China;* orcid.org/0000-0002-2179-9507

Complete contact information is available at: https://pubs.acs.org/10.1021/acs.nanolett.4c05540

### Author Contributions

[¶]M.N. and R.-L.M. contributed equally to this work.

### Notes

The authors declare no competing financial interest.

## ■ ACKNOWLEDGMENTS

This work was supported by the National Natural Science Foundation of China (Grants Nos. 92165207, 12474490, 12074368, 12034018, and 92265113) and the Innovation Program for Quantum Science and Technology (Grant No. 2021ZD0302300), and this work was partially carried out at the USTC Center for Micro and Nanoscale Research and Fabrication. H.-W.J. and X.H. acknowledge financial support by U.S. ARO through Grant No. W911NF2310016 and No. W911NF2310018, respectively. X.X. acknowledges European Union's Horizon 2020 research and innovation programme under the Grant Agreement No. 951852 (QLSI project).

## ■ REFERENCES

(1) Veldhorst, M.; Hwang, J. C. C.; Yang, C. H.; Leenstra, A. W.; de Ronde, B.; Dehollain, J. P.; Muhonen, J. T.; Hudson, F. E.; Itoh, K. M.; Morello, A.; et al. An addressable quantum dot qubit with fault-tolerant control-fidelity. *Nat. Nanotechnol.* **2014**, *9* (12), 981−985.

(2) Muhonen, J. T.; Dehollain, J. P.; Laucht, A.; Hudson, F. E.; Kalra, R.; Sekiguchi, T.; Itoh, K. M.; Jamieson, D. N.; McCallum, J. C.; Dzurak, A. S.; et al. Storing quantum information for 30 seconds in a nanoelectronic device. *Nat. Nanotechnol.* **2014**, *9* (12), 986−991.

(3) Zhang, X.; Li, H.-O.; Cao, G.; Xiao, M.; Guo, G.-C.; Guo, G.-P. Semiconductor quantum computation. *Nat. Sci. Rev.* **2019**, *6* (1), 32−54.

(4) Burkard, G.; Ladd, T. D.; Pan, A.; Nichol, J. M.; Petta, J. R. Semiconductor spin qubits. *Rev. Mod. Phys.* **2023**, *95* (2), 025003.

(5) Petit, L.; Eenink, H. G. J.; Russ, M.; Lawrie, W. I. L.; Hendrickx, N. W.; Philips, S. G. J.; Clarke, J. S.; Vandersypen, L. M. K.; Veldhorst, M. Universal quantum logic in hot silicon qubits. *Nature* **2020**, *580* (7803), 355−359.

(6) Yang, C. H.; Leon, R. C. C.; Hwang, J. C. C.; Saraiva, A.; Tanttu, T.; Huang, W.; Camirand Lemyre, J.; Chan, K. W.; Tan, K. Y.; Hudson, F. E.; et al. Operation of a silicon quantum processor unit cell above one kelvin. *Nature* **2020**, *580* (7803), 350−354.

(7) Zwerver, A. M. J.; Krähenmann, T.; Watson, T. F.; Lampert, L.; George, H. C.; Pillarisetty, R.; Bojarski, S. A.; Amin, P.; Amitonov, S. V.; Boter, J. M.; et al. Qubits made by advanced semiconductor manufacturing. *Nat. Electro.* **2022**, *5* (3), 184−190.

(8) Gonzalez-Zalba, M. F.; de Franceschi, S.; Charbon, E.; Meunier, T.; Vinet, M.; Dzurak, A. S. Scaling silicon-based quantum computing using CMOS technology. *Nat. Electro.* **2021**, *4* (12), 872−884.

(9) Xue, X.; Patra, B.; van Dijk, J. P. G.; Samkharadze, N.; Subramanian, S.; Corna, A.; Paquelet Wuetz, B.; Jeon, C.; Sheikh, F.; Juarez-Hernandez, E.; et al. CMOS-based cryogenic control of silicon quantum circuits. *Nature* **2021**, *593* (7858), 205−210.

(10) Johnson, M. A. I.; Mądzik, M. T.; Hudson, F. E.; Itoh, K. M.; Jakob, A. M.; Jamieson, D. N.; Dzurak, A.; Morello, A. Beating the Thermal Limit of Qubit Initialization with a Bayesian Maxwell's Demon. *Phys. Rev. X* **2022**, *12* (4), 041008.

(11) Oakes, G. A.; Ciriano-Tejel, V. N.; Wise, D. F.; Fogarty, M. A.; Lundberg, T.; Lainé, C.; Schaal, S.; Martins, F.; Ibberson, D. J.; Hutin, L.; et al. Fast High-Fidelity Single-Shot Readout of Spins in Silicon Using a Single-Electron Box. *Phys. Rev. X* **2023**, *13* (1), 011023.

(12) Mills, A. R.; Guinn, C. R.; Feldman, M. M.; Sigillito, A. J.; Gullans, M. J.; Rakher, M. T.; Kerckhoff, J.; Jackson, C. A. C.; Petta, J. R. High-Fidelity State Preparation, Quantum Control, and Readout of an Isotopically Enriched Silicon Spin Qubit. *Phys. Rev. Appl.* **2022**, *18* (6), 064028.

(13) Huang, J. Y.; Su, R. Y.; Lim, W. H.; Feng, M.; van Straaten, B.; Severin, B.; Gilbert, W.; Dumoulin Stuyck, N.; Tanttu, T.; Serrano, S.; et al. High-fidelity spin qubit operation and algorithmic initialization above 1 K. *Nature* **2024**, *627* (8005), 772−777.

(14) Harvey-Collard, P.; D'Anjou, B.; Rudolph, M.; Jacobson, N. T.; Dominguez, J.; Ten Eyck, G. A.; Wendt, J. R.; Pluym, T.; Lilly, M. P.; Coish, W. A.; et al. High-Fidelity Single-Shot Readout for a Spin Qubit via an Enhanced Latching Mechanism. *Phys. Rev. X* **2018**, *8* (2), 021046.

(15) Urdampilleta, M.; Niegemann, D. J.; Chanrion, E.; Jadot, B.; Spence, C.; Mortemousque, P.-A.; Bäuerle, C.; Hutin, L.; Bertrand, B.; Barraud, S.; et al. Gate-based high fidelity spin readout in a CMOS device. *Nat. Nanotechnol.* **2019**, *14* (8), 737−741.

(16) Yoneda, J.; Takeda, K.; Otsuka, T.; Nakajima, T.; Delbecq, M. R.; Allison, G.; Honda, T.; Kodera, T.; Oda, S.; Hoshi, Y.; et al. A quantum-dot spin qubit with coherence limited by charge noise and fidelity higher than 99.9%. *Nat. Nanotechnol.* **2018**, *13* (2), 102−106.

(17) Yang, C. H.; Chan, K. W.; Harper, R.; Huang, W.; Evans, T.; Hwang, J. C. C.; Hensen, B.; Laucht, A.; Tanttu, T.; Hudson, F. E.; et al. Silicon qubit fidelities approaching incoherent noise limits via pulse engineering. *Nat. Electro.* **2019**, *2* (4), 151−158.

(18) Xue, X.; Russ, M.; Samkharadze, N.; Undseth, B.; Sammak, A.; Scappucci, G.; Vandersypen, L. M. K. Quantum logic with spin qubits crossing the surface code threshold. *Nature* **2022**, *601* (7893), 343−347.

(19) Noiri, A.; Takeda, K.; Nakajima, T.; Kobayashi, T.; Sammak, A.; Scappucci, G.; Tarucha, S. Fast universal quantum gate above the fault-tolerance threshold in silicon. *Nature* **2022**, *601* (7893), 338−342.

(20) Mills, A. R.; Guinn, C. R.; Feldman, M. M.; Sigillito, A. J.; Gullans, M. J.; Rakher, M. T.; Kerckhoff, J.; Jackson, C. A. C.; Petta, J. R. High-Fidelity State Preparation, Quantum Control, and Readout of an Isotopically Enriched Silicon Spin Qubit. *Phys. Rev. Appl.* **2022**, *18* (6), 064028.

(21) Mądzik, M. T.; Asaad, S.; Youssry, A.; Joecker, B.; Rudinger, K. M.; Nielsen, E.; Young, K. C.; Proctor, T. J.; Baczewski, A. D.; Laucht, A.; et al. Precision tomography of a three-qubit donor quantum processor in silicon. *Nature* **2022**, *601* (7893), 348−353.

(22) Takeda, K.; Noiri, A.; Nakajima, T.; Kobayashi, T.; Tarucha, S. Quantum error correction with silicon spin qubits. *Nature* **2022**, *608* (7924), 682−686.

(23) Preskill, J. Quantum Computing in the NISQ era and beyond. *Quantum* **2018**, *2*, 79.

(24) Mills, A. R.; Zajac, D. M.; Gullans, M. J.; Schupp, F. J.; Hazard, T. M.; Petta, J. R. Shuttling a single charge across a one-dimensional array of silicon quantum dots. *Nat. Commun.* **2019**, *10* (1), 1063.

(25) Yoneda, J.; Huang, W.; Feng, M.; Yang, C. H.; Chan, K. W.; Tanttu, T.; Gilbert, W.; Leon, R. C. C.; Hudson, F. E.; Itoh, K. M.; et al. Coherent spin qubit transport in silicon. *Nat. Commun.* **2021**, *12* (1), 4114.

(26) Noiri, A.; Takeda, K.; Nakajima, T.; Kobayashi, T.; Sammak, A.; Scappucci, G.; Tarucha, S. A shuttling-based two-qubit logic gate for linking distant silicon quantum processors. *Nat. Commun.* **2022**, *13* (1), 5740.

(27) Zwerver, A. M. J.; Amitonov, S. V.; de Snoo, S. L.; Mądzik, M. T.; Rimbach-Russ, M.; Sammak, A.; Scappucci, G.; Vandersypen, L. M. K. Shuttling an Electron Spin through a Silicon Quantum Dot Array. *PRX Quantum* **2023**, *4* (3), 030303.

(28) Loss, D.; DiVincenzo, D. P. Quantum computation with quantum dots. *Phys. Rev. A* **1998**, *57* (1), 120−126.

(29) Kandel, Y. P.; Qiao, H.; Fallahi, S.; Gardner, G. C.; Manfra, M. J.; Nichol, J. M. Coherent spin-state transfer via Heisenberg exchange. *Nature* **2019**, *573* (7775), 553−557.
(30) Abrams, D. M.; Didier, N.; Johnson, B. R.; Silva, M. P. d.; Ryan, C. A. Implementation of XY entangling gates with a single calibrated pulse. *Nat. Electro.* **2020**, *3* (12), 744−750.
(31) Petta, J. R.; Johnson, A. C.; Taylor, J. M.; Laird, E. A.; Yacoby, A.; Lukin, M. D.; Marcus, C. M.; Hanson, M. P.; Gossard, A. C. Coherent Manipulation of Coupled Electron Spins in Semiconductor Quantum Dots. *Science* **2005**, *309* (5744), 2180−2184.
(32) He, Y.; Gorman, S. K.; Keith, D.; Kranz, L.; Keizer, J. G.; Simmons, M. Y. A two-qubit gate between phosphorus donor electrons in silicon. *Nature* **2019**, *571* (7765), 371−375.
(33) Kalra, R.; Laucht, A.; Hill, C. D.; Morello, A. Robust Two-Qubit Gates for Donors in Silicon Controlled by Hyperfine Interactions. *Phys. Rev. X* **2014**, *4* (2), 021044.
(34) Sigillito, A. J.; Gullans, M. J.; Edge, L. F.; Borselli, M.; Petta, J. R. Coherent transfer of quantum information in a silicon double quantum dot using resonant SWAP gates. *npj Quantum Inf.* **2019**, *5* (1), 110.
(35) Nowack, K. C.; Shafiei, M.; Laforest, M.; Prawiroatmodjo, G. E. D. K.; Schreiber, L. R.; Reichl, C.; Wegscheider, W.; Vandersypen, L. M. K. Single-Shot Correlations and Two-Qubit Gate of Solid-State Spins. *Science* **2011**, *333* (6047), 1269−1272.
(36) Brunner, R.; Shin, Y. S.; Obata, T.; Pioro-Ladriere, M.; Kubo, T.; Yoshida, K.; Taniyama, T.; Tokura, Y.; Tarucha, S. Two-Qubit Gate of Combined Single-Spin Rotation and Interdot Spin Exchange in a Double Quantum Dot. *Phys. Rev. Lett.* **2011**, *107* (14), 146801.
(37) Petit, L.; Russ, M.; Eenink, G. H. G. J.; Lawrie, W. I. L.; Clarke, J. S.; Vandersypen, L. M. K.; Veldhorst, M. Design and integration of single-qubit rotations and two-qubit gates in silicon above one Kelvin. *Commun. Mater.* **2022**, *3* (1), 82.
(38) Heinz, I.; Burkard, G. Crosstalk analysis for single-qubit and two-qubit gates in spin qubit arrays. *Phys. Rev. B* **2021**, *104* (4), 045420.
(39) Veldhorst, M.; Yang, C. H.; Hwang, J. C. C.; Huang, W.; Dehollain, J. P.; Muhonen, J. T.; Simmons, S.; Laucht, A.; Hudson, F. E.; Itoh, K. M.; et al. A two-qubit logic gate in silicon. *Nature* **2015**, *526* (7573), 410−414.
(40) Zhang, X.; Hu, R.-Z.; Li, H.-O.; Jing, F.-M.; Zhou, Y.; Ma, R.-L.; Ni, M.; Luo, G.; Cao, G.; Wang, G.-L.; et al. Giant Anisotropy of Spin Relaxation and Spin-Valley Mixing in a Silicon Quantum Dot. *Phys. Rev. Lett.* **2020**, *124* (25), 257701.
(41) Zhang, X.; Zhou, Y.; Hu, R.-Z.; Ma, R.-L.; Ni, M.; Wang, K.; Luo, G.; Cao, G.; Wang, G.-L.; Huang, P.; et al. Controlling Synthetic Spin-Orbit Coupling in a Silicon Quantum Dot with Magnetic Field. *Phys. Rev. Appl.* **2021**, *15* (4), 044042.
(42) Hu, R.-Z.; Ma, R.-L.; Ni, M.; Zhou, Y.; Chu, N.; Liao, W.-Z.; Kong, Z.-Z.; Cao, G.; Wang, G.-L.; Li, H.-O.; et al. Flopping-mode spin qubit in a Si-MOS quantum dot. *Appl. Phys. Lett.* **2023**, *122* (13), 134002.
(43) Yang, C. H.; Rossi, A.; Lai, N. S.; Leon, R.; Lim, W. H.; Dzurak, A. S. Charge state hysteresis in semiconductor quantum dots. *Appl. Phys. Lett.* **2014**, *105* (18), 183505.
(44) Elzerman, J. M.; Hanson, R.; Willems van Beveren, L. H.; Witkamp, B.; Vandersypen, L. M. K.; Kouwenhoven, L. P. Single-shot read-out of an individual electron spin in a quantum dot. *Nature* **2004**, *430* (6998), 431−435.
(45) Huang, W.; Yang, C. H.; Chan, K. W.; Tanttu, T.; Hensen, B.; Leon, R. C. C.; Fogarty, M. A.; Hwang, J. C. C.; Hudson, F. E.; Itoh, K. M.; et al. Fidelity benchmarks for two-qubit gates in silicon. *Nature* **2019**, *569* (7757), 532−536.
(46) Veldhorst, M.; Ruskov, R.; Yang, C. H.; Hwang, J. C. C.; Hudson, F. E.; Flatte, M. E.; Tahan, C.; Itoh, K. M.; Morello, A.; Dzurak, A. S. Spin-orbit coupling and operation of multivalley spin qubits. *Phys. Rev. B* **2015**, *92* (20), 201401.
(47) Ferdous, R.; Chan, K. W.; Veldhorst, M.; Hwang, J. C. C.; Yang, C. H.; Sahasrabudhe, H.; Klimeck, G.; Morello, A.; Dzurak, A. S.; Rahman, R. Interface-induced spin-orbit interaction in silicon quantum dots and prospects for scalability. *Phys. Rev. B* **2018**, *97* (24), 241401.
(48) Ruskov, R.; Veldhorst, M.; Dzurak, A. S.; Tahan, C. Electron g-factor of valley states in realistic silicon quantum dots. *Phys. Rev. B* **2018**, *98* (24), 245424.
(49) Yoneda, J.; Otsuka, T.; Takakura, T.; Pioro-Ladrière, M.; Brunner, R.; Lu, H.; Nakajima, T.; Obata, T.; Noiri, A.; Palmstrøm, C. J.; et al. Robust micromagnet design for fast electrical manipulations of single spins in quantum dots. *Appl. Phys. Express* **2015**, *8* (8), 084401.
(50) Kawakami, E.; Scarlino, P.; Ward, D. R.; Braakman, F. R.; Savage, D. E.; Lagally, M. G.; Friesen, M.; Coppersmith, S. N.; Eriksson, M. A.; Vandersypen, L. M. K. Electrical control of a long-lived spin qubit in a Si/SiGe quantum dot. *Nat. Nanotechnol.* **2014**, *9*, 666.
(51) Leon, R. C. C.; Yang, C. H.; Hwang, J. C. C.; Camirand Lemyre, J.; Tanttu, T.; Huang, W.; Huang, J. Y.; Hudson, F. E.; Itoh, K. M.; Laucht, A.; et al. Bell-state tomography in a silicon many-electron artificial molecule. *Nat. Commun.* **2021**, *12* (1), 3228.
(52) Cifuentes, J. D.; Tanttu, T.; Gilbert, W.; Huang, J. Y.; Vahapoglu, E.; Leon, R. C. C.; Serrano, S.; Otter, D.; Dunmore, D.; Mai, P. Y.; et al. Bounds to electron spin qubit variability for scalable CMOS architectures. *Nat. Commun.* **2024**, *15* (1), 4299.
(53) Laucht, A.; Kalra, R.; Muhonen, J. T.; Dehollain, J. P.; Mohiyaddin, F. A.; Hudson, F.; McCallum, J. C.; Jamieson, D. N.; Dzurak, A. S.; Morello, A. High-fidelity adiabatic inversion of a P-31 electron spin qubit in natural silicon. *Appl. Phys. Lett.* **2014**, *104* (9), 092115.
(54) Ni, M.; Ma, R.-L.; Kong, Z.-Z.; Chu, N.; Liao, W.-Z.; Zhu, S.-K.; Wang, C.; Luo, G.; Liu, D.; Cao, G.; et al. Correcting on-chip distortion of control pulses with silicon spin qubits. *Chin. Phys. B* **2025**, *34* (1), 010308.
(55) Watson, T. F.; Philips, S. G. J.; Kawakami, E.; Ward, D. R.; Scarlino, P.; Veldhorst, M.; Savage, D. E.; Lagally, M. G.; Friesen, M.; Coppersmith, S. N.; et al. A programmable two-qubit quantum processor in silicon. *Nature* **2018**, *555* (7698), 633−637.
(56) McKay, D. C.; Wood, C. J.; Sheldon, S.; Chow, J. M.; Gambetta, J. M. Efficient Z gates for quantum computing. *Phys. Rev. A* **2017**, *96* (2), 022330.
(57) Sung, Y.; Ding, L.; Braumüller, J.; Vepsäläinen, A.; Kannan, B.; Kjaergaard, M.; Greene, A.; Samach, G. O.; McNally, C.; Kim, D.; et al. Realization of High-Fidelity CZ and ZZ-Free iSWAP Gates with a Tunable Coupler. *Phys. Rev. X* **2021**, *11* (2), 021058.
(58) Hofmann, H. F. Complementary Classical Fidelities as an Efficient Criterion for the Evaluation of Experimentally Realized Quantum Operations. *Phys. Rev. Lett.* **2005**, *94* (16), 160504.
(59) Politi, A.; Cryan, M. J.; Rarity, J. G.; Yu, S.; O'Brien, J. L. Silica-on-Silicon Waveguide Quantum Circuits. *Science* **2008**, *320* (5876), 646−649.
(60) Kha, A.; Joynt, R.; Culcer, D. Do micromagnets expose spin qubits to charge and Johnson noise? *Appl. Phys. Lett.* **2015**, *107* (17), 172101.
(61) Keith, D.; Gorman, S. K.; He, Y.; Kranz, L.; Simmons, M. Y. Impact of charge noise on electron exchange interactions in semiconductors. *npj Quantum Inf.* **2022**, *8* (1), 17.
(62) Dial, O. E.; Shulman, M. D.; Harvey, S. P.; Bluhm, H.; Umansky, V.; Yacoby, A. Charge Noise Spectroscopy Using Coherent Exchange Oscillations in a Singlet-Triplet Qubit. *Phys. Rev. Lett.* **2013**, *110* (14), 146804.


https://doi.org/10.1021/acs.nanolett.4c05540
*Nano Lett.* 2025, 25, 3766−3772